# Genetically encoded fluorescent sensors adapted to acidic pH highlight subdomains within the plant cell apoplast

Hortense Moreau, Isabelle Gaillard, Nadine Paris

# Genetically encoded fluorescent sensors adapted to acidic pH highlight subdomains within the plant cell apoplast.

Hortense Moreau, Isabelle Gaillard and Nadine Paris.

BPMP, Univ Montpellier, CNRS, INRAE, Montpellier SupAgro, Montpellier, France

hortense.moreau@supagro.fr

isabelle.gaillard@inrae.fr

nadine.paris@cnrs.fr

**Highlight**

Using genetically encoded tandems of fluorescent proteins optimized for acidic pH measurement, we show that the apoplast is a complex environment regarding sensor coverage with pH heterogeneity in pavement cells.

**Abstract**

Monitoring pH is one of the challenges in understanding diverse physiological regulations as well as ionic balance, especially in highly acidic environments such as the apoplast and the vacuole. To circumvent the poor efficiency of pH measurements below pH 5, we designed three genetically encoded sensors composed of two fluorescent proteins in tandem. We selected fluorescent protein couples of low but sufficiently different pKa so that each protein could differentially sense the imposed pH. The generated tandems, named Acidin2, Acidin3 and Acidin4, were produced in *E. coli* and extensively characterized. Altogether, these generated tandems cover a pH range of 3-8. The Acidins were targeted either for release in the apoplast (Apo) or for anchoring at the outer face of the plasma membrane (PM-Apo), with the fluorescent part exposed in the apoplast. Apoplastic Acidins in stably transformed *Arabidopsis thaliana* primary roots responded immediately and reversibly to pH changes, directly reporting physiological conditions related to cell elongation. In addition, membrane-anchored Acidins reveal a gradual acidification from the surface through the anticlinal wall of pavement cells, a process controlled at least partially by P-ATPase activity.

**Keywords**

root, acid growth, apoplast, biosensor, fluorescence, live imaging, pH

## Introduction

Measuring pH in real time is essential to understanding plant development and adaptation to environmental changes. At the cellular level, the tightly regulated pH of endomembrane compartments is used to control functional protein trafficking (Martinière *et al.*, 2013; Dragwidge *et al.*, 2019), especially in the lumen of the trans-Golgi network/early endosome (TGN/EE). This network operates as a sorting platform at the intersection of the vacuolar/secretion/endocytosis pathways, with a luminal steady state pH of 5.32 (Dragwidge *et al.*, 2019) under constant remodeling (Shimizu *et al.*, 2021). The pH also plays a central role in controlling cell elongation. Based on the 'acid growth theory', auxin triggers a transient acidification of the apoplast that in turn leads to the activation of enzymes such as expansins with an optimal activity at pH 4. The activity of expansin leads to an increase in cell wall extensibility to allow turgor pressure-mediated cell expansion (Rayle and Cleland, 1992). Regarding cell wall pH, a model of negative feedback was recently proposed for switching cell elongation on and off that involves two hormone peptides with antagonistic actions on $H^+$-ATPase activity. The acidifying 'plant peptide containing sulfated tyrosine 1' (PSY1) interacts with the receptor kinase PSY1R and triggers phosphorylation of the auto-inhibitory loop of $H^+$-ATPase (Amano *et al.*, 2007; Fuglsang *et al.*, 2014), while the rapid alkalinization factor (RALF) binds the *Catharanthus roseus* RLK1-LIKE cell receptor kinase FERONIA, indirectly leading to the inhibition of $H^+$-ATPase (Pearce *et al.*, 2001). Interestingly, PSY1 not only promotes cell elongation through its direct effect on $H^+$-ATPase, but also induces the transcription of some RALFs that can trigger a response cascade resulting in the inactivation of $H^+$-ATPase and, consequently, the inhibition of cell elongation (Gjetting *et al.*, 2020). This complex switch illustrates how pH homeostasis is tightly regulated in elongation, and exemplifies the need to monitor apoplastic pH in living tissue with cellular to subcellular definition and no restrictions on the acidic range.

As for the TGN/EE lumen, a deeper understanding of the role of pH in these highly dynamic processes in cell elongation has been limited by technical deficiencies that prevent accurate measurements in the acidic range, below pH 5. External *in vivo* pH measurements were originally

achieved using $H^+$ microelectrodes in *Arabidopsis thaliana* (Staal *et al.*, 2011) and maize (Peters and Felle, 1999), and more recently with fluorescent dyes (Han and Burgess, 2010). The lowest published pH values in plants have been obtained in leaves (Geilfus and Mühling, 2012) and within the root apoplast (Martinière *et al.*, 2018) using the fluorescent probe Oregon Green (pKa 4.6), which is functional down to pH 2.5. However, this probe is rapidly internalized in root tip cells if it is not coupled to dextran. When Oregon Green was covalently attached to the cellulose binding domain (CBD) peptide from *Clostridium cellulovorans* cellulase, local cell wall acidification was reported (down to pH 4.3) in the root central elongation zone that was submitted to gravitropism (Fasano *et al.*, 2001). The probe 8-hydroxypyrene-1,3,6-trisulfonic acid (HPTS) has also been successfully used to monitor apoplastic pH in the root transition/elongation zone and has enabled studies of root expansion at the cellular level (Barbez *et al.*, 2017). Unfortunately, HPTS poorly penetrates the apoplast, resulting in transient labeling with limited sensitivity below pH 5.5 (Martinière *et al.*, 2018). Regarding genetically encoded fluorescent probes, ratiometric pHluorin has successfully been used in plants (Miesenböck *et al.*, 1998), especially in the secretory pathway (Martinière *et al.*, 2013) and at the plasma membrane (PM), where it is well-tolerated (Martinière *et al.*, 2018) In order to further expand the performance of sensors in the acidic pH range, tandems of fluorescent proteins with various pH sensitivities have been developed. As an example of such tandem-based fluorescent sensors, pHusion (Gjetting *et al.*, 2012) has been successfully used in the plant endomembrane system (Luo *et al.*, 2015). This sensor is composed of a monomeric red fluorescent protein (mRFP) fused to an enhanced green fluorescent protein (EGFP), allowing pH measurements in the range of 4.5-8.

Here, we have designed new sensors adapted to acidic pH, similar to the recently published tandem pHlemon (Burgstaller *et al.*, 2019) that is comprised of the pH-insensitive mTurquoise2 in the neutral pH range and the pH-sensitive enhanced yellow fluorescent protein (EYFP). For our sensors, we selected proteins with a low pKa, including: Tag blue fluorescent protein (TagBFP; pKa 2.7) from *Entacmaea quadricolor* (Subach *et al.*, 2011); Gamillus (pKa 3.4), isolated from the jellyfish *Olindias*

*formosus* (Shinoda *et al.*, 2018); and the synthetic yellow fluorescent protein 2 (SYFP2; pKa 6), a moderate acid-sensitive yellow protein derived from the *Aequorea victoria* GFP, mVenus (Kremers *et al.*, 2006). These fluorescent proteins were fused to mRFP (Campbell *et al.*, 2002) to generate three tandem biosensors that we have named Acidins. The properties of these Acidins were extensively analyzed by spectrofluorometry and confocal microscopy. Together with the formerly described pHluorin, the Acidins extend our ability to measure pH changes from pH 3 to pH 8. The Acidins targeted to the apoplast with either a transmembrane domain (TMD) or a signal peptide responded rapidly and reversibly to *in vivo* pH changes, and allowed the fine measurement of pH in the transition zone with regard to cell elongation and the gravitropic response. Surprisingly, PM-associated Acidins revealed a gradual acidification from the surface of the epidermis towards the internal, anticlinal region of pavement cells that is at least partially mediated by $H^+$-ATPase. Our study therefore presents three new sensors that can be used to explore *in vivo* apoplastic pH variation with regard to cell elongation, a highly dynamic process.

## Materials and Methods

### Constructs

An optimized version of TagBFP2 for plant and *E. coli* codon usage (Subach *et al.*, 2011) was synthesized by GenCust. Fluorescent proteins were obtained using previously published sequences for SYFP2 (Kremers *et al.*, 2006), mRFP1 (Campbell *et al.*, 2002), and Gamillus (Shinoda *et al.*, 2018), in which the two predicted N-glycosylation sites were removed by point mutation (N129Q and N213Q). To make the Acidin tandems, the mRFP1 sequence was fused at its N-terminus to TagBFP2 for Acidin2, Gamillus for Acidin3, and SYFP2 for Acidin4, along with the linker Gly-Ser for Acidin2 and Ala-Val-Asn-Ala for Acidin3 and Acidin4. The Apo and PM-Apo Acidins were generated as previously described (Martinière *et al.*, 2018), except for the signal peptide from LuPME1 (Al-Qsous *et al.*, 2004) that was used for the Apo versions. Sensors were assembled using the Golden Braid cloning method

(Sarrion-Perdigones *et al.*, 2013) and were placed under the control of either a 35S promoter or the UBQ10 promoter (Grefen *et al.*, 2010). For production in *E. coli*, a HIS-tag was added at the N-terminus of the Acidins by cloning the coding sequence between the Nco1 and Xho1 sites of pRset B in place of pHluorin (Martinière *et al.*, 2018).

**Plant material**

For expression in plants, Acidin constructs were introduced in the *Agrobacterium tumefaciens* strain EHA105 that was used either for infiltration of 4-week-old *Nicotiana tabacum* cv. SR1 leaves as previously described (Brandizzi *et al.*, 2002), or to generate *Arabidopsis thaliana* ecotype Columbia-8 stable transformants according to the floral dip method (Clough and Bent, 1998).

***In vitro* characterization and calibration**

After production in *E. coli* (strain BL21 PlysS), recombinant Acidin3 and Acidin4 were purified in a nickel column following the manufacturer's instructions while Acidin2 was used without further purification. Different sets of 100 mM pH buffers were used for *in vitro* and *in situ* calibration, including: acetic acid/glycine for pH 2.5 and 3; acetic acid/Bis-tris propane (BTP) for pH values from 3.5 to 5; 2-(N-morpholino)ethanesulfonic acid (MES)/BTP for pH values from 5.5 to 6.5; and 4-(2-hydroxyethyl)-1-piperazineethanesulfonic acid (HEPES)/BTP for pH values from 7 to 8.5. The *in vitro* characterization was performed on a Xenius spectrofluorometer (SAFA) with recombinant Acidins diluted 1/1000 in pH buffers and the following settings: 405 nm Exc./450-500 nm Em. for TagBFP2; 476 nm Exc./504-550 nm Em. for Gamillus; 561 nm Exc./580 to 650 nm Em. for mRFP; and 488 nm Exc./510-554 nm Em. for SYFP2. FRET was evaluated under a confocal microscope using the lambda scan mode with 5-nm steps after excitation at 405 nm, 488 nm or 514 nm for Acidin2, Acidin3 and Acidin4, respectively.

For *in situ* calibration under the confocal microscope, 5 µl of Acidin produced in bacteria were diluted 1/10 to 1/20 with the pH buffers, applied on a coverslip, and imaged with the same settings used for plant material imaging. For *in vivo* calibration with a ratiometric microscope, half-strength MS medium was added to the plant material with 100 mM glycine HCl for pH 2 and 3, or 100 mM MES KOH for pH 4, 5 and 6. For *in vivo* calibration under a confocal microscope, the same 100 mM buffers used for *in vitro* characterization were complemented with 150 mM KCl and 20 µM nigericin and infiltrated in tobacco leaves 30 to 60 min prior to observation.

The obtained ratios were plotted as a function of pH with a Boltzmann equation to fit sigmoidal curves using the GraphPad Prism software as previously described (Martinière *et al.*, 2013, 2018).

**Immunoblot and immunofluorescence**

For western blot analysis, the Acidins were detected using anti-RFP antibodies (6G6, Chromotek 1/2000). The orientation of the PM-Apo versions was confirmed by immunofluorescence on intact tobacco protoplasts as previously described (Martinière *et al.*, 2012). The fusion PIP2.1-mCherry was used as a negative control, and the red fluorescent protein was detected with anti-DsRed antibodies (Takara 1/500) and anti-rabbit Alexa Fluor 488 F(ab)'2 antibodies (Fisher 1/500).

**Growing conditions**

Arabidopsis seeds were sterilized and stratified for 2 days prior to growth in half-strength MS medium supplemented with 2.5 mM MES-KOH (pH 6), 1% sucrose and 0.8% (w/v) agar (Sigma A4675). Plates were placed vertically in a growth chamber on a 16-h:8-h light:dark cycle at 21°C with 70% relative humidity and a light intensity of 200 $\mu mol \cdot m^{-2} \cdot s^{-1}$ for 4 days.

**Confocal microscopy and epifluorescence ratio imaging**

Prior to observation of Arabidopsis roots, plantlets were transferred on to microscopy slides covered with a thin layer (1-2 mm) of half-strength MS medium and 0.8% (w/v) phytagel, and were returned to the growth chamber for another 24 h. At least one hour before imaging with a confocal microscope, the glass slide covered with medium was removed from the plate, excess medium was removed, and a coverslip was placed on the root portion of the 5-day-old seedlings.

Confocal observations were made with a Leica SP8 inverted microscope using a 40× water objective (HCX Plan Apochromat CS 1.1 N.A.). The average laser output in the defocused beam for 100% AOTF was 0.49 mW, 1.01 mW, 1.15 mW and 3.07 mW for the 405 nm, 488 nm, 514 nm and 561 nm lines, respectively. The same Exc./Em. settings used for *in vitro* characterization were applied for imaging except that 488 nm Exc. was used for Gamillus. Z-series were generated with 1-µm steps to explore up to 20-50 µm in depth of the plant tissue at the highest setting possible but still below saturation. The xz projection was calculated using Fiji software. For the gravitropism response, plantlets on slides were turned 90° for 30 min before imaging. The overall time that one plantlet remained in the horizontal position for observation did not exceed 10 min.

Direct ratiometric imaging was performed using a Zeiss Axiovert 200M inverted fluorescence microscope equipped with a shutter Lambda 10-B external wheel, by sequential illumination with a 10X/0.3 NA Plan Neofluoar objective. For Acidin2, a LedHub source was used for excitation at 385 nm or with a 550/20 filter; emission was collected with 480/40 and 600/50 emission filters for TagBFP2 and mRFP, respectively. Images (binning 2 parameters) were acquired using a CDD camera (CoolSNAP HQ; Photometrics) with the MetaFluor ratio imaging software.

Ratiometric images were generated using Fiji software by dividing the images of the two channels after manually applying a threshold.

**Statistics**

For each condition or treatment, two biological replicates were made and 5-10 focal planes, images or time series were taken. Statistical analyses were performed with GraphPad Prism software using Student's t-test ($P<0.05$ was considered to be a significant difference). Unless specified in the legend, data are expressed as mean ± SEM.

**Results**

**The Acidins are broad-range pH sensors**

We generated three tandems of fluorescent proteins, RFP-TagBFP2, RFP-Gamillus and RFP-SYFP2, and named them Acidin2, Acidin3 and Acidin4, respectively (Fig. 1A, C and E). The sensors were produced in bacteria (Fig. S1) and characterized *in vitro*. As expected, the two fluorescent proteins that compose a tandem differed in their response amplitudes to pH, shown for the highest and lowest pH covered by the respective Acidin (Fig. 1A, C and E), or for the entire range of analyzed pH levels (Fig. S2). For each Acidin and pHluorin, the fluorescence ratio was calculated and plotted as a function of pH either before (Fig. S3) or after normalization with the lowest value set to 1 (Fig. 1B, D, F and G). The resulting Acidin curves fit a sigmoidal curve ($R^2$ ranging from 0.96 to 0.99) and cover a pH range from 3-6.5 (2.5 pH units below the pH coverage of pHluorin) with some overlap (Fig. 1H). We also tested *in vitro* the impact of cations and redox-active compounds on the Acidins and found little to no impact, at least on the fluorescence ratio, for Acidin 2 and Acidin4 (Fig. S4A and C). In contrast, exchanging $Cl^-$ with $NO_3^-$ affected the fluorescence ratio with a 50% increase for both Acidin2 and Acidin4 (Fig. S4B) at 100mM concentration. It is important to note that this ionic concentration tested is far beyond the native values that are in the mM range (Mühling and Sattelmacher, 1995; Sattelmacher, 2001; Mühling and Läuchli, 2002; Dreyer *et al.*, 2017). We also tested the ability of the sensors to generate internal FRET and found that all three Acidins presented

an apparent energy transfer leading to mRFP fluorescence that is independent of pH for Acidin2 and Acidin4 (Fig. S5).

Next, we generated two apoplastic forms of Acidins (Fig. S6): one named PM-Apo (Fig. 2B), which is anchored in the PM thanks to a long TMD, as previously described (Martinière *et al.*, 2018); and Apo (Fig. 3B), a secreted form released into the external medium. After transient expression in tobacco epidermal cells, the different labelling patterns were observed by confocal microscopy. Similar to the control pHluorin, the three PM-Apo Acidins were detected along the entire periphery of the cell, as shown on one focal plane (Fig. 2A) out of the corresponding z-series presented in Fig. S7. Acidins were correctly associated with the PM as expected (Fig. 2B) and were uncleaved, as shown by the exclusive localization at the PM (Fig. 2C, arrow) in addition to Hechtian strands after plasmolysis, for both fluorescent proteins composing the sensor. The apoplastic orientation of the pH-sensing moiety of PM-Apo Acidins was supported by the type of amino acids composing the TMD (Lorent *et al.*, 2020) and by previous proteinase K protection assays on its pHluorin equivalent (Martinière *et al.*, 2018). This was reinforced by immunofluorescence on intact protoplasts (Fig. 2D-E), since the RFP part of the Acidin fusion was detected by antibodies on the outside of the protoplast (Fig. 2D, green), while the negative control fusion made of the aquaporin PIP2.1 fused to a red fluorescent tag facing the cytosol was not immunodetected (Fig. 2E). For the secreted Apo Acidins, the fluorescence signal shown for one focal plane out of a z-series (Fig. S8) was detected in limited portions of the cells (Fig. 3A), as for the previously published pHluorin version (Fig. 3A, arrowhead) (Martinière *et al.*, 2018), with a covering that appears to decrease as sensor pKa increases. After plasmolysis, fluorescent signal from the two proteins composing the sensor was detected in the entire space between cells (Fig. 3C-E) and not at the PM (arrows), supporting a release of the sensor in the apoplast. To conclude, the three Acidins are correctly expressed and localized in plant cell apoplasts and are well-tolerated by the plant secretory pathway with the exception of Apo-Acidin3, which that is partially mislocalized in the vacuole (Fig. S8).

**The apoplast pH decreases from the surface to the inside of the epidermis**

Upon careful inspection of the fluorescence pattern for PM-Apo-expressing epidermal cells, we found a combination of magenta and cyan signals that varied with the focal plane. We collected z-series covering the entire thickness of the epidermis and performed a z projection (Fig. 4). While a predominance of TagBFP2 signal (cyan) was found in the anticlinal portion of the epidermis (Fig. 4B, star), more mRFP signal (magenta) was found in the periclinal regions for PM-anchored Acidin in the anticlinal view (Fig. 4B). In contrast to PM-Apo, Apo Acidins were detected almost exclusively in some curved portion of the cells, and the magenta signal dominated with little heterogeneity (Fig. 4C). The z projection analysis revealed that fluorescence signal was restricted to the periclinal portion of the apoplast (Fig. 4D). The difference in signal distribution of PM-Apo and Apo in z is summarized in Fig. 4E.

As suggested by comparing Figures 2A and 3A with their ratiometric equivalent (Figs. S7 and S8), the relative difference of fluorescence intensity for the two channels is indicative of pH variation. To further quantify pH variation through the epidermis thickness, we first selected regions of interest (ROI) from single focal planes representative of the labelling pattern for PM-Apo and Apo fusions (Fig. S9) and calculated the pH using to *in situ* calibration (Fig. 1B). The resulting pH analyzed from a large pool of data showed a differential distribution of pH between the two apoplastic sensors (Fig. 4F), with an average pH of 3.8 (n=533) for the PM-anchored sensor and pH 4.5 (n=554) for a freely diffusing sensor (difference of $p<0.0001$ in an unpaired t-test). Next, we quantified the pH starting from a z projection of tobacco epidermis expressing PM-Apo-Acidin2. For this, we collected fluorescence signal from the surface down to 8 µm towards the anticlinal wall (Fig. S10A). Clamping at various pH levels led to signal (Fig. S10B-D) and ratio (Fig. S10E) homogeneity in the z dimension. In contrast, the distribution of TagBFP2 and mRFP signal in the epidermis thickness was heterogenous in untreated conditions (Fig. S11A and Supplemental Movies 1 and 2), with undulated

portions presenting more mRFP than line areas. As a consequence, the fluorescence ratio gradually decreased from the surface down to the anticlinal region of the epidermis (Figs. 5A and Fig. S11B). The pH values were then calculated (Fig. 5B) using an *in vivo* calibration curve from clamping in z (Fig. 5C). Starting from the surface down to 5 µm, the pH value was found to gradually decrease, remaining stable at pH 4.2 deep in the anticlinal region (Fig. 5D). Subsequently, we investigated the role of $H^+$-ATPases in this pH heterogeneity, for which we modified the activity of the PM proton pump by applying fusicoccin. This fungal toxin is known to stabilize the activating complex between 14-3-3 proteins and PM $H^+$-ATPase and therefore is expected to lead to an increase in proton release in the apoplast. Upon the action of fusicoccin, the overall pH values dropped in the entire thickness of the epidermis, with a decrease of 1.5 pH units at the surface and 0.5 pH units deep in the anticlinal wall (Fig. 5B, D), suggesting that $H^+$-ATPase is involved in building this pH gradient. In contrast to the region beyond 5 µm, the outer apoplast was very different between straight and undulated regions, with ratio values over the range of the pH calibration in the undulation and control conditions (Fig. S11B). In contrast to clamping (Fig. S10E), the gradient is not entirely compromised with fusicoccin. Given that the toxin constitutively activates the PM ATPase, this suggests that other parameters such as the distribution of PM $H^+$-ATPase or local cell wall composition may also be involved in the observed gradient in pavement cells.

**Acidin allows the fine measurement of apoplastic pH in growing roots**

Since plant tissue growth is believed to involve local and transient acidification (Barbez *et al.*, 2017), plant research could benefit from sensors that are more sensitive in the acidic pH range, such as the Acidins. We thus generated stable Arabidopsis lines expressing PM-Apo and Apo Acidins. With the exception of Acidin3-expressing plants, which presented some fluorescence mislocalization in the vacuole as well as in epidermal cells (Fig. S8), Acidin2- and Acidin4-based sensors displayed clear and robust labelling in roots (Fig. 6) and cotyledons (Fig. S12). As shown on two focal planes (Fig. 6A-B)

and the corresponding z-series from Arabidopsis root tip comprising half of the root (Fig. 6C), PM-Apo-Acidin4 labelling was found on the entire cell periphery (Fig. 6E). In contrast to PM-Apo, the Apo labelling was more discontinuous and appeared to be concentrated in pockets that were clearly visible in the z projection (Fig. 6F-H). With the exception of the region covered by the root cap (Supplemental Movie 3), no signal was detected at the surface of the epidermis, suggesting that the Apo sensor diffused away from the root, as illustrated in Figure 6J.

Next, we evaluated pH in primary roots expressing Apo-Ac2 (Fig. 7A, C) or PM-Apo-Ac2 (Fig. 7B-C). As shown on ratiometric images and the corresponding longitudinal ratiometric profiles (Fig. 7C), we observed: an acidic zone at the level of the root cap (RC); a more alkaline zone in the meristem; and a gradual acidification starting in the transition zone (TZ) that expands to the elongation zone (EZ), as expected from previously published data (Staal *et al.*, 2011). Growth media buffered at various pH values were successively applied to the Apo-Ac2 seedlings while monitoring the fluorescence ratio in real-time. As shown in Figure 7D, the pH-related ratio in the TZ changed instantaneously, stabilized in less than one minute, and could be reversed (Supplemental Movie 4). The corresponding longitudinal ratiometric profiles at different pH levels were plotted in Figure 7E and compared. While the effect of the applied pH on the ratio is greater in the meristem and the TZ than in the EZ, the calibration curves from the different regions of the root fit a sigmoidal curve and presented a pKa close to that obtained *in situ* (Fig. S13). This suggests that the *in vivo* pH clamping was effective and allowed pH measurement in the apoplast of living primary roots expressing Apo-Ac2. From 90 to 180 µm, the profile of untreated primary roots (Fig. 7E, black) almost overlaps with the profile at pH 5 (Fig. 7E, red), meaning that the observed root ratio varies from 1.3 to 1.1 along the different zones for the same pH. Using the calibration curve in the corresponding zone (Fig. S13), the calculated apoplastic pH in primary root is 5.4 in the lower meristem, 5 in the transition zone, and 4.6 in the elongation zone.

Since the pH estimated in the primary roots was at the upper limit of the Acidin2 detection range, we switched to Acidin4 to further analyze the TZ zone. Gradual acidification was observed in a detailed confocal view covering the end of the TZ in Arabidopsis roots expressing PM-Apo-Ac4 (Fig. 8A-B). We measured the pH along the longitudinal axis at the interface of two epidermal cell lines (Fig. 8A, arrows and Fig. S14) and plotted the corresponding values (Fig. 8C) using *in situ* calibration (Fig. 1F). Three zones could be identified: Z1, starting from the end of the meristem up to where cells start to elongate and pH is stable (pH 5.2); Z2, where cells doubled their length as compared to their width, with a gradual pH acidification (average pH 5); and Z3, a zone where epidermal cells continued their elongation with pH remaining stable at pH 4.7 (Fig. 8B-C). The link between root growth and apoplastic pH was also confirmed by applying a pH 3 buffer on Apo-Acidin2-expressing roots, resulting in an instantaneous growth increase (Fig. S15, Supplemental Movie 5).

To test the ability of Acidin to detect pH modification in auxin-related growth, we analyzed the pH upon eliciting a gravitropism response in PM-Apo-Acidin4 primary roots (Fig. 8D-E). As described in previous reports (Monshausen *et al.*, 2011; Barbez *et al.*, 2017), we observed a significant alkalinization of the root tip inner face when compared to the outer face (pH 5.35 versus pH 5.2, $p<0.0001$; Figs. 8E and S14) or the control root tip (pH 5.3 on both faces).

**Discussion**

In this work, we described and extensively characterized the novel genetically encoded bimolecular fluorescent sensors Acidin2, Acidin3 and Acidin4, which were designed to extend our ability to monitor pH towards the acidic range in living tissue. We chose to assemble two fluorescent proteins in tandem with low but different pKa values, to ensure that they would not be equally affected by low pH while remaining fluorescent. Indeed, this is what was observed with recombinant Acidins, allowing the acquisition of typical sigmoid ratiometric pH curves. Interestingly, the pKa of the Acidins

observed *in vitro* turned out to be very close to the mean of the known pKa of the two fluorescent proteins composing the tandem, suggesting that this approach could be expanded to other fluorescent proteins with low pKa. The robustness of measuring pH using an *in situ* calibration method with recombinant Acidin was effectively illustrated by *in vivo* calibration on tobacco pavement cells expressing Acidin2 anchored in the PM (Fig. 5C), where the pKa (4.3) is very close to the pKa measured by *in situ* calibration (4.4). In contrast, the pKa obtained *in vivo* on the root tip with a free Acidin2 was slightly lower (3.4) regardless of the region observed (Fig. S13). This observation illustrates that there is no general rule for empirically determining the best calibration. Nevertheless, whichever calibration or sensor used, we obtained the same absolute pH of 5 in primary root TZ (Figs. S13B and 8C), suggesting that there is no buffering effect of the sensor itself. Altogether, the three Acidins covered a range of pH that extended 2.5 pH units below the minimum of most available fluorescent pH probes, including pHluorin, with an interesting overlap. Although Acidin3 was capable of functioning *in vitro*, its partial vacuolar localization *in planta* (Figs. 3A and S8C) suggests a trafficking problem in the plant secretory pathway. Since Acidin2 and Acidin4 were well-tolerated, this could be due to some structural features of Gamillus, which have only been tested in human cells so far (Shinoda *et al.*, 2018), or to the removal of N-glycosylation sites that was performed in this work (see Materials and Methods section).

The large majority of pH values that we measured in Arabidopsis root tips using our Acidin sensors were in the range of pH 4.5 to 5.5. This fits well with previously published data using either HPTS (Barbez *et al.*, 2017) or Oregon Green coupled to a cellulose-binding domain (Fasano *et al.*, 2001). Our results on the transition zone support the hypothesis that a decrease of half a pH unit is sufficient for switching to an elongating status. Three zones were identified in the distal meristem, based on their pH profile: Z1, where the pH was stable at 5.2; Z2, where gradual pH acidification was observed (average pH 5); and Z3, where the pH remained stable at 4.7 (Fig. 8C). Interestingly, acidification zone Z2 is narrow (less than 100 µm) and corresponds to cells that are already twice as long as they are wide, suggesting that acidification in the apoplast occurs after elongation has

already begun, as previously reported using HPTS (Barbez *et al.*, 2017). Although it is clear that apoplastic pH is linked to cell elongation, this appears to contradict the chronology of the acid growth theory, a model mainly supported by experiments on aerial tissue (Fendrych *et al.*, 2016), in which cell wall acidification triggers a cascade of events that ultimately lead to cell wall loosening and subsequent cell elongation. Further analysis of the chronology between acidification and elongation will require monitoring pH from single cells, which could be achieved by expressing the Acidins under cell line-specific promoters (Marquès-Bueno *et al.*, 2016) and dynamic imaging, since pH is known to oscillate in primary roots (Monshausen *et al.*, 2011). The fast and reversible reactivity of Acidins also makes them promising as monitors of physiological events associated with fast and massive acidification of the apoplast, such as during gravitropism (Monshausen *et al.*, 2011), or upon contact with a *Fusarium oxysporum* elicitor in roots (Kesten *et al.*, 2019). It could also be interesting to use the Acidins in highly acidic environments, such as in grape berries where pH values can be as low as 2.5 at the green stage (Fontes *et al.*, 2011).

In this work, we localized our sensors to the apoplast either in a freely diffusing form (Apo) or anchored in the PM (PM-Apo), and we obtained different distribution patterns (Figs. 4E, 6E and 6J). The ability of the Apo form to diffuse is supported by the fact that the outer face of the epidermis is labelled only when a cuticle is present, i.e. in pavement cells or in the root cap (Berhin *et al.*, 2019). Nevertheless, some areas of the apoplast remained unlabeled, including the anticlinal region of the leaf epidermis. Although we cannot exclude that this reflects the difference in wall thickness, especially at the outer lobe/neck interface (Bidhendi *et al.*, 2020), one possible explanation for the uneven distribution of Apo is a limited diffusion due to heterogeneity in cell wall porosity. This hypothesis is supported by the size of the Acidins, assuming they are globular proteins (53 Å), as compared to the estimated size of the pores, 30-50 Å (Carpita *et al.*, 1979). The heterogeneity of apoplast porosity in pavement cells is also supported by recent results from elegant tools designed to monitor microviscosity, using boron-dipyrromethene (BODIPY)-based rigidochromic molecular rotors that were localized to the PM or to the cell wall (Michels *et al.*, 2020). Previous observations

showing that microviscosity is decreased in the pectin-impaired mutant *quasimodo* (Michels *et al.*, 2020) and that BSA diffusion in cell walls depends on the degree of pectin methylation (Willats *et al.*, 2001) support the hypothesis that Apo diffusion could be affected by cell wall composition. In contrast to Apo, the PM-Apo is evenly distributed in the cell periphery but does show heterogeneity in pH in tobacco leaf pavement cells as well as in Arabidopsis cotyledons, as previously described using HPTS (Barbez *et al.*, 2017). In both tissues, the pH in the anticlinal region is more acidic than in the periclinal region (Fig. 5). This could be related to the extreme complexity of jigsaw cell growing processes, where variation in relative growth rates has been observed in leaves (Elsner *et al.*, 2018) as well as in cotyledons (Armour *et al.*, 2015).

The fact that this pH gradient is abolished upon nigericin treatment and compromised by fusicoccin suggests that active ion and proton exchanges are involved in its formation. Given that fusicoccin constitutively activates ATPase, the incomplete impairment of the pH gradient could be explained by the uneven distribution of $H^+$-ATPase along the thickness of the epidermis, as observed in pollen tubes (Hoffmann *et al.*, 2020) but also suggested in the "local acidification theory" for the optimized uptake of iron from the rhizosphere (Martín-Barranco *et al.*, 2020). Interestingly, the gradient is even more pronounced in the curved region of pavement cells. The formation of interdigitating undulations is extremely complex and has been extensively studied, including recently (Liu *et al.*, 2021; Igisch *et al.*, 2022). The resulting structure includes a specific organization of cortical actin and microtubule cytoskeletons as well as a distinct distribution of methylated and demethylated pectins that have different mechanical properties, with the latter being proposed to transmit ROP6-mediated indentation formation (Malivert *et al.*, 2021; Lin *et al.*, 2022; Tang *et al.*, 2022). Interestingly, labelling with COS488, a probe for demethylated homogalacturonan (Mravec *et al.*, 2014), suggests that demethylated pectin is more concentrated in the neck periclinal wall, which appears to bulge out above the lobe side (Bidhendi *et al.*, 2019, 2020). Since demethylated pectin is highly negatively charged, it would be interesting to further study its impact on the Acidin2 fluorescence ratio which is higher in the neck than the lobe face of the periclinal region (Fig. 5A,

undulation). This intriguing observation suggests that Acidin2 could be useful for monitoring not only pH but also a subpopulation of the pectin cell wall, with regard to cell shape determination (Altartouri *et al.*, 2019; Haas *et al.*, 2020).

Our results therefore highlight an unexpected complexity of the apoplast, along with the existence of a pH gradient in the anticlinal wall of pavement cells. The difference in signal distribution between PM-Apo and Apo also suggests that these two apoplastic sensors most likely report pH from only partially overlapping territories. The possibility of assessing apoplastic pH at a cellular resolution with PM-anchored Acidin, which can report pH closer to the membrane, will open new perspectives in the study of the acid growth theory in root tissue. This will be a marked improvement over probes such as HPTS, which remain at the surface of the root (Barbez *et al.*, 2017; Li *et al.*, 2021).

**Acknowledgments**

We thank the "plateforme d'histocytologie et d'imagerie cellulaire végétale" (PHIV) and the Montpellier ressources imagerie (MRI) platform for access to microscopes.

**Author contribution**

All three authors contributed equally to this work.

**Conflict of interest**

The authors have no conflicts to declare.

**Funding statement**

This work was funded by the Homeowall project ANR-20-CE11-0008 from the Agence Nationale de la Recherche (ANR). HM is the recipient of a PhD fellowship (2018-2021) from the Institut National de Recherche pour l'Agriculture, l'Alimentation et l'Environnement (INRAE) and from the Occitanie region (PROTOMICS contract #24001128-P2194).

**Data availability**

The data supporting the findings of this study are available from the corresponding author, Nadine Paris, upon request.

**Bibliography**

**Al-Qsous S, Carpentier E, Klein-Eude D, Burel C, Mareck A, Dauchel H, Gomord V, Balangé AP**. 2004. Identification and isolation of a pectin methylesterase isoform that could be involved in flax cell wall stiffening. Planta **219**, 369–378.

**Altartouri B, Bidhendi AJ, Tani T, Suzuki J, Conrad C, Chebli Y, Liu N, Karunakaran C, Scarcelli G, Geitmann A**. 2019. Pectin Chemistry and Cellulose Crystallinity Govern Pavement Cell Morphogenesis in a Multi-Step Mechanism. Plant Physiology **181**, 127–141.

**Amano Y, Tsubouchi H, Shinohara H, Ogawa M, Matsubayashi Y**. 2007. Tyrosine-sulfated glycopeptide involved in cellular proliferation and expansion in Arabidopsis. Proceedings of the National Academy of Sciences **104**, 18333–18338.

**Armour WJ, Barton DA, Law AMK, Overall RL**. 2015. Differential Growth in Periclinal and Anticlinal Walls during Lobe Formation in Arabidopsis Cotyledon Pavement Cells. The Plant Cell **27**, 2484–2500.

**Barbez E, Dünser K, Gaidora A, Lendl T, Busch W**. 2017. Auxin steers root cell expansion via apoplastic pH regulation in Arabidopsis thaliana. Proceedings of the National Academy of Sciences **114**, E4884–E4893.

**Berhin A, de Bellis D, Franke RB, Buono RA, Nowack MK, Nawrath C**. 2019. The root cap cuticle: a cell wall structure for seedling establishment and lateral root formation. Cell **176**, 1367-1378.e8.

**Bidhendi AJ, Altartouri B, Gosselin FP, Geitmann A**. 2019. Mechanical Stress Initiates and Sustains the Morphogenesis of Wavy Leaf Epidermal Cells. Cell Reports **28**, 1237-1250.e6.

**Bidhendi A j., Chebli Y, Geitmann A**. 2020. Fluorescence visualization of cellulose and pectin in the primary plant cell wall. Journal of Microscopy **278**, 164–181.

**Brandizzi F, Frangne N, Marc-Martin S, Hawes C, Neuhaus J-M, Paris N**. 2002. The Destination for Single-Pass Membrane Proteins Is Influenced Markedly by the Length of the Hydrophobic Domain. The Plant Cell **14**, 1077–1092.

**Burgstaller S, Bischof H, Gensch T, *et al.*** 2019. pH-Lemon, a fluorescent protein-based pH reporter for acidic compartments. ACS sensors **4**, 883–891.

**Campbell RE, Tour O, Palmer AE, Steinbach PA, Baird GS, Zacharias DA, Tsien RY**. 2002. A monomeric red fluorescent protein. Proceedings of the National Academy of Sciences **99**, 7877–

7882.

**Carpita N, Sabularse D, Montezinos D, Delmer DP**. 1979. Determination of the pore size of cell walls of living plant cells. Science **205**, 1144–1147.

**Clough SJ, Bent AF**. 1998. Floral dip: a simplified method for Agrobacterium-mediated transformation ofArabidopsis thaliana. The Plant Journal **16**, 735–743.

**Dragwidge JM, Scholl S, Schumacher K, Gendall AR**. 2019. NHX-type Na+(K+)/H+ antiporters are required for TGN/EE trafficking and endosomal ion homeostasis in Arabidopsis thaliana. Journal of Cell Science **132**, jcs226472.

**Dreyer I, Gomez-Porras JL, Riedelsberger J**. 2017. The potassium battery: a mobile energy source for transport processes in plant vascular tissues. New Phytologist **216**, 1049–1053.

**Elsner J, Lipowczan M, Kwiatkowska D**. 2018. Differential growth of pavement cells of Arabidopsis thaliana leaf epidermis as revealed by microbead labeling. American Journal of Botany **105**, 257–265.

**Fasano JM, Swanson SJ, Blancaflor EB, Dowd PE, Kao T, Gilroy S**. 2001. Changes in root cap pH are required for the gravity response of the Arabidopsis root. The Plant Cell **13**, 907–921.

**Fendrych M, Leung J, Friml J**. 2016. TIR1/AFB-Aux/IAA auxin perception mediates rapid cell wall acidification and growth of Arabidopsis hypocotyls (G Stacey, Ed.). eLife **5**, e19048.

**Fontes N, Gerós H, Delrot S**. 2011. Grape Berry Vacuole: A Complex and Heterogeneous Membrane System Specialized in the Accumulation of Solutes. American Journal of Enology and Viticulture **62**, 270–278.

**Fuglsang AT, Kristensen A, Cuin TA, *et al.*** 2014. Receptor kinase-mediated control of primary active proton pumping at the plasma membrane. The Plant Journal: For Cell and Molecular Biology **80**, 951–964.

**Geilfus C-M, Mühling KH**. 2012. Transient alkalinization in the leaf apoplast of Vicia faba L. depends on NaCl stress intensity: an in situ ratio imaging study. Plant, Cell & Environment **35**, 578–587.

**Gjetting SK, Mahmood K, Shabala L, Kristensen A, Shabala S, Palmgren M, Fuglsang AT**. 2020. Evidence for multiple receptors mediating RALF-triggered Ca2+ signaling and proton pump inhibition. The Plant Journal **104**, 433–446.

**Gjetting SK, Ytting CK, Schulz A, Fuglsang AT**. 2012. Live imaging of intra- and extracellular pH in plants using pHusion, a novel genetically encoded biosensor. Journal of Experimental Botany **63**, 3207–3218.

**Grefen C, Donald N, Hashimoto K, Kudla J, Schumacher K, Blatt MR**. 2010. A ubiquitin-10 promoter-based vector set for fluorescent protein tagging facilitates temporal stability and native protein distribution in transient and stable expression studies. The Plant Journal **64**, 355–365.

**Haas KT, Wightman R, Meyerowitz EM, Peaucelle A**. 2020. Pectin homogalacturonan nanofilament expansion drives morphogenesis in plant epidermal cells. Science **367**, 1003–1007.

**Han J, Burgess K**. 2010. Fluorescent indicators for intracellular pH. Chemical Reviews **110**, 2709–2728.

**Hoffmann RD, Portes MT, Olsen LI, *et al.*** 2020. Plasma membrane H+-ATPases sustain pollen tube growth and fertilization. Nature Communications **11**, 2395.

**Igisch CP, Miège C, Jaillais Y**. 2022. Cell shape: A ROP regulatory tug-of-war in pavement cell morphogenesis. Current Biology **32**, R116–R118.

**Kesten C, Gámez-Arjona FM, Scholl S, *et al.*** 2019. Pathogen-induced pH changes regulate the growth-defense balance of plants. bioRxiv, 550491.

**Kremers G-J, Goedhart J, van Munster EB, Gadella TWJ**. 2006. Cyan and Yellow Super Fluorescent Proteins with Improved Brightness, Protein Folding, and FRET Förster Radius,. Biochemistry **45**, 6570–6580.

**Li L, Verstraeten I, Roosjen M, *et al.*** 2021. Cell surface and intracellular auxin signalling for H+ fluxes in root growth. Nature **599**, 273–277.

**Lin W, Tang W, Pan X, Huang A, Gao X, Anderson CT, Yang Z**. 2022. Arabidopsis pavement cell morphogenesis requires FERONIA binding to pectin for activation of ROP GTPase signaling. Current biology: CB **32**, 497–507.

**Liu S, Jobert F, Rahneshan Z, Doyle SM, Robert S**. 2021. Solving the Puzzle of Shape Regulation in Plant Epidermal Pavement Cells. Annual Review of Plant Biology **72**, 525–550.

**Lorent JH, Levental KR, Ganesan L, Rivera-Longsworth G, Sezgin E, Doktorova M, Lyman E, Levental I**. 2020. Plasma membranes are asymmetric in lipid unsaturation, packing and protein shape. Nature Chemical Biology **16**, 644–652.

**Luo Y, Scholl S, Doering A, *et al.*** 2015. V-ATPase activity in the TGN/EE is required for exocytosis and recycling in Arabidopsis. Nature Plants **1**, 1–10.

**Malivert A, Erguvan Ö, Chevallier A, Dehem A, Friaud R, Liu M, Martin M, Peyraud T, Hamant O, Verger S**. 2021. FERONIA and microtubules independently contribute to mechanical integrity in the Arabidopsis shoot. PLOS Biology **19**, e3001454.

**Marquès-Bueno MM, Morao AK, Cayrel A, Platre MP, Barberon M, Caillieux E, Colot V, Jaillais Y, Roudier F, Vert G**. 2016. A versatile Multisite Gateway-compatible promoter and transgenic line collection for cell type-specific functional genomics in Arabidopsis. The Plant Journal **85**, 320–333.

**Martín-Barranco A, Spielmann J, Dubeaux G, Vert G, Zelazny E**. 2020. Dynamic Control of the High-Affinity Iron Uptake Complex in Root Epidermal Cells1. Plant Physiology **184**, 1236–1250.

**Martinière A, Bassil E, Jublanc E, Alcon C, Reguera M, Sentenac H, Blumwald E, Paris N**. 2013. In vivo intracellular pH measurements in tobacco and Arabidopsis reveal an unexpected pH gradient in the endomembrane system. The Plant Cell **25**, 4028–4043.

**Martinière A, Gibrat R, Sentenac H, Dumont X, Gaillard I, Paris N**. 2018. Uncovering pH at both sides of the root plasma membrane interface using noninvasive imaging. Proceedings of the National

Academy of Sciences **115**, 6488–6493.

**Martinière A, Lavagi I, Nageswaran G, *et al.*** 2012. Cell wall constrains lateral diffusion of plant plasma-membrane proteins. Proceedings of the National Academy of Sciences **109**, 12805–12810.

**Michels L, Gorelova V, Harnvanichvech Y, Borst JW, Albada B, Weijers D, Sprakel J**. 2020. Complete microviscosity maps of living plant cells and tissues with a toolbox of targeting mechanoprobes. Proceedings of the National Academy of Sciences **117**, 18110–18118.

**Miesenböck G, De Angelis DA, Rothman JE**. 1998. Visualizing secretion and synaptic transmission with pH-sensitive green fluorescent proteins. Nature **394**, 192–195.

**Monshausen GB, Miller ND, Murphy AS, Gilroy S**. 2011. Dynamics of auxin-dependent Ca2+ and pH signaling in root growth revealed by integrating high-resolution imaging with automated computer vision-based analysis. The Plant Journal: For Cell and Molecular Biology **65**, 309–318.

**Mravec J, Kračun SK, Rydahl MG, *et al.*** 2014. Tracking developmentally regulated post-synthetic processing of homogalacturonan and chitin using reciprocal oligosaccharide probes. Development **141**, 4841–4850.

**Mühling KH, Läuchli A**. 2002. Determination of apoplastic Na+ in intact leaves of cotton by in vivo fluorescence ratio-imaging. Functional plant biology : FPB.

**Mühling KH, Sattelmacher B**. 1995. Apoplastic ion concentration of intact leaves of field bean (Vicia faba) as influenced by ammonium and nitrate nutrition. Journal of Plant Physiology **147**, 81–86.

**Pearce G, Moura DS, Stratmann J, Ryan CA**. 2001. RALF, a 5-kDa ubiquitous polypeptide in plants, arrests root growth and development. Proceedings of the National Academy of Sciences of the United States of America **98**, 12843–12847.

**Peters WS, Felle HH**. 1999. The correlation of profiles of surface pH and elongation growth in Maize roots. Plant Physiology **121**, 905–912.

**Rayle DL, Cleland RE**. 1992. The Acid Growth Theory of auxin-induced cell elongation is alive and well. Plant Physiology **99**, 1271–1274.

**Sarrion-Perdigones A, Vazquez-Vilar M, Palací J, Castelijns B, Forment J, Ziarsolo P, Blanca J, Granell A, Orzaez D**. 2013. GoldenBraid 2.0: A Comprehensive DNA Assembly Framework for Plant Synthetic Biology. Plant Physiology **162**, 1618–1631.

**Sattelmacher B**. 2001. The apoplast and its significance for plant mineral nutrition. New Phytologist **149**, 167–192.

**Shimizu Y, Takagi J, Ito E, *et al.*** 2021. Cargo sorting zones in the trans -Golgi network visualized by super-resolution confocal live imaging microscopy in plants. Nature Communications **12**, 1901.

**Shinoda H, Ma Y, Nakashima R, Sakurai K, Matsuda T, Nagai T**. 2018. Acid-Tolerant Monomeric GFP from Olindias formosa. Cell Chemical Biology **25**, 330-338.e7.

**Staal M, Cnodder TD, Simon D, Vandenbussche F, Straeten DVD, Verbelen J-P, Elzenga T,**

**Vissenberg K**. 2011. Apoplastic alkalinization is instrumental for the inhibition of cell elongation in the Arabidopsis root by the ethylene precursor 1-aminocyclopropane-1-carboxylic acid. Plant Physiology **155**, 2049–2055.

**Subach OM, Cranfill PJ, Davidson MW, Verkhusha VV**. 2011. An Enhanced Monomeric Blue Fluorescent Protein with the High Chemical Stability of the Chromophore. PLOS ONE **6**, e28674.

**Tang W, Lin W, Zhou X, Guo J, Dang X, Li B, Lin D, Yang Z**. 2022. Mechano-transduction via the pectin-FERONIA complex activates ROP6 GTPase signaling in Arabidopsis pavement cell morphogenesis. Current biology: CB **32**, 508–517.

**Willats WGT, Orfila C, Limberg G, *et al.*** 2001. Modulation of the degree and pattern of methyl-esterification of pectic homogalacturonan in plant cell walls. Journal of Biological Chemistry **276**, 19404–19413.

**Legends**

**Figure 1: Schematic representation and *in vitro* characterization of Acidins**

Acidin2 (A and B), Acidin3 (C and D) and Acidin4 (E and F) are genetically encoded tandems of fluorescent proteins made with mRFP (pKa 4.5) fused respectively to TagBFP2 (pKa 2.7), Gamillus (pKa 3.4), or SYFP2 (pKa 6) by a GS or AVNA linker. The Acidins were produced in *E. coli*, and their responses to pH were analyzed.

A, C and E: Emission profiles of the fluorescent proteins in Acidins at the highest (dashed line) or lowest pH (solid line) in the linear range of pH sensing. These values correspond to pH 5 and 2.5 for Acidin2, pH 5.5 and 2.5 for Acidin3, and pH 7 and pH 4.5 for Acidin4. Profiles obtained by spectrofluorometry are expressed in arbitrary units relative to the optimum and set to 1 for each fluorescent protein composing the tandem.

B, D, F and G: pH calibration curves for the three Acidins are represented as fluorescence ratios at the excitation wavelength ratios 561 nm/405 nm (B), 561 nm/488 nm (D), 514 nm/561 nm (F) and 496 nm/476 nm (G). Ratios obtained with a confocal are expressed relative to the minimum and set to 1 (see Fig. S3 for the raw data and details).

H: Normalized *in vitro* calibration curves of Acidins in comparison to pHluorin, fit with sigmoidal curves (Acidin2: $R^2$ = 0.95, pKa = 4.4; Acidin3: $R^2$ = 0.96, pKa = 4.5; Acidin4: $R^2$ = 0.99, pKa = 5.6; and pHluorin: $R^2$ = 0.99, pKa = 6.8). Data are transformed into the range 0-1 by Min-Max normalization.

**Figure 2: Localization of PM-anchored Acidins in tobacco epidermal cells**

Tobacco epidermal cells were transiently transformed with pH sensors anchored in the PM. Cells were then analyzed after three days of expression with a confocal microscope.

A: Merge images showing the expression pattern of PM-Apo with either Acidin2, Acidin3, Acidin4 or

pHluorin.

B: Schematic representation of the Acidin fusion protein PM-Apo.

C: Cells expressing PM-Apo-Acidin2 were submitted to plasmolysis with 2% NaCl for 30 min prior to observation.

D and E: Living tobacco protoplasts expressing either PM-Apo-Acidin2 (D) or the PM protein aquaporin PIP2.1 tagged on its cytoplasmic side with mCherry (E) were immunolabelled with rabbit primary anti-DsRed antibodies and secondary anti-rabbit Alexa Fluor 488 F(ab)'2 antibodies. In red: fluorescence emitted from either mRFP (D) or mCherry (E). In green: fluorescence signal resulting from immunolabelling was detected only for the PM-Apo-Acidin2 fusion (D), confirming the exposure of mRFP on the outside of the protoplast.

Cyan: fluorescence signal from TagBFP for Acidin2, Gamillus for Acidin3, SYFP2 for Acidin4, or 476Exc for pHluorin. Magenta: fluorescence signal from mRFP for the Acidins, or the 496Exc channel for pHluorin. Arrow: PM. Scale bar: 10 µm.

**Figure 3: Localization of free-diffusing apoplastic Acidins in tobacco epidermal cells**

Tobacco epidermal cells were transiently transformed with pH sensors released in the apoplast. Then, after three days of expression, cells were analysed with a confocal microscope.

A: Merge images showing the expression pattern of Apo with either Acidin2, Acidin3, Acidin4, or pHluorin.

B: Schematic representation of the Acidin fusion protein Apo.

C-E: Cells expressing either Apo-Acidin2 (C), Apo-Acidin3 (D) or Apo-Acidin4 (E) were submitted to plasmolysis with NaCl 2% for 30 min prior to observation.

Cyan: fluorescence signal from TagBFP for Acidin2, Gamillus for Acidin3, SYFP2 for Acidin4, or 476Exc for pHluorin. Magenta: fluorescence signal from mRFP for the Acidins, or the 496Exc channel for pHluorin. Arrowhead: labeled apoplast. Arrow: PM. Scale bar: 10 µm.

**Figure 4: Acidins reveal the existence of apoplastic subdomains with different pH values in tobacco epidermal cells**

Tobacco leaves transiently transformed with the sensor PM-Apo-Acidin2 (A and B) or Apo-Acidin2 (C and D) were observed under a confocal microscope. Series of confocal images were taken through the thickness of the epidermis from which a single focal plane is presented in a periclinal view (A and C) or an anticlinal view (B and D). The solid yellow line indicates the ROI from which the z projection was performed, whereas the dashed yellow line indicates the focal plane from which the respective periclinal view originated.

E: Schematic z projection of fluorescence labelling in pavement cell epidermis for PM-anchored (PM-Apo) and freely diffusing (Apo) forms of apoplastic fusions. PM-Apo labels the entire thickness of the epidermal PM, whereas Apo is restricted to the periclinal part of the apoplast.

F: Histograms of pH distribution collected from periclinal views for PM-Apo-Acidin2 (n = 568) or Apo-Acidin2 (n = 552).

False color: cyan for the TagBFP2 signal and magenta for the mRFP signal. Stars indicate the middle of the epidermal layer. Scale bar: 10 µm.

**Figure 5: PM $H^+$-ATPase is involved in the acidification of the apoplast through pavement cell thickness**

Tobacco leaves transiently transformed with the sensor PM-Apo-Acidin2 were observed under a

confocal microscope. Series of confocal images were taken through the thickness of the epidermis and z projections were generated in either undulated or straight regions of the cell periphery.

A: Ratiometric images of an anticlinal view in straight (line) or undulated (undulation) regions of pavement cells. The dashed white line indicates the zero position from which fluorescence data were collected for pH quantification through the epidermis thickness.

B: pH profile from the anticlinal-periclinal intersection (zero) up to 10 µm into the cell layer in straight (red) or undulated (blue) regions with (dashed line) or without (solid line) treatment with 10 µM fusicoccin.

C: *In vivo* calibration curve obtained from the z projection after clamping with nigericin at various pH levels.

D: Effect of fusicoccin on pH in the anticlinal region of the epidermis (5 to 10 µm from the surface). n=27; ANOVA followed by Tukey's test; $p<0.05$ between a and b groups.

Scale bar: 10 µm.

**Figure 6: Localization of Acidins in Arabidopsis primary root tip apoplast**

Primary roots from 5- to 6-day-old Arabidopsis seedlings expressing PM-Apo-Acidin4 (A-C) or Apo-Acidin2 (F-H) were observed with a confocal microscope.

A-B: Confocal merge images at a focal plane in the median section with high (A) or low (B) laser power.

C-D: Z projection in the transition zone of a PM-Apo-Acidin4 root (C) or an untransformed root at the same settings (D).

F-G: Confocal merge images at two different focal planes of the same root; see also Supplemental

Movie 3 for the entire z-series.

H-I: Z projection in the transition zone of Apo-Acidin2 roots (H) or untransformed roots at the same settings (I).

E and J: Schematic z projections of the fluorescence pattern in primary roots for PM-anchored (PM-Apo; E) and freely diffusing (Apo; J) forms of apoplastic fusions showing that PM-Apo equally labels all cell layers, whereas Apo is accumulated in pockets between cells and can be detected at the surface of the epidermis only when the root cap cell layer is present.

c: cap cell layer; e: epidermis; co: cortex. Scale bar: 10 µm.

**Figure 7: Ratio of fluorescence monitoring and *in vivo* calibration in Arabidopsis root tips**

Arabidopsis plants were stably transformed with PM-Apo-Acidin2 and Apo-Acidin2 and fluorescence was observed in the primary roots of 5- to 6-day-old seedlings using ratiometric imaging.

A and B: Ratiometric images in false color of the first 400 µm (apical part) of primary root tips expressing either Apo-Acidin2 (A) or PM-Apo-Acidin2 (B).

C: Typical ratiometric profiles, with high values corresponding to high pH (n = 7 for Apo-Acidin2 and n = 3 for PM-Apo-Acidin2).

D and E: 561 nm/405 nm fluorescence ratio over time in the transition zone (D) or in the first 400 µm of the root expressing Apo-Acidin2 after equilibration (E) and perfusion with unbuffered half-strength MS, and then successively with half-strength MS buffered at various pH (100 mM glycine-HCl for pH 2 and pH 3, or 100 mM MES-KOH 0.1M for pH 4 to pH 6). See also Supplemental Movie 4.

RC: root cap; TZ: transition zone: EZ: elongation zone. Scale bar: 10 µm.

**Figure 8: pH variations monitored in living Arabidopsis primary roots expressing Acidins are associated with cell elongation**

Arabidopsis plants were stably transformed with PM-Apo-Acidin4 and fluorescence was observed in the primary roots of 5- to 6-day-old seedlings using a confocal microscope.

A and B: Ratiometric image from a 300-µm portion of the epidermis in the transition zone of a primary root tip (A) and the corresponding pH profile (B) from the intercellular portion delimited by arrows in A.

C: Measures of pH in the three zones identified in B ($pH_{Z1}$ = 5.1, n = 2,971; $pH_{Z2}$ = 5, n = 2,102; $pH_{Z3}$ = 4.6, n = 2,675, p<0.0001).

D: Ratiometric images of root tips from 5- to 6-day-old seedlings maintained in normal conditions (Control) or submitted to a 90° rotation for 25 to 30 min (Gravi).

E: pH measured in the epidermal cell layer at the outer and inner sides of the root after gravistimulation or at the left and right sides for the control root (n = 1,022 to 1,328, p<0.0001).

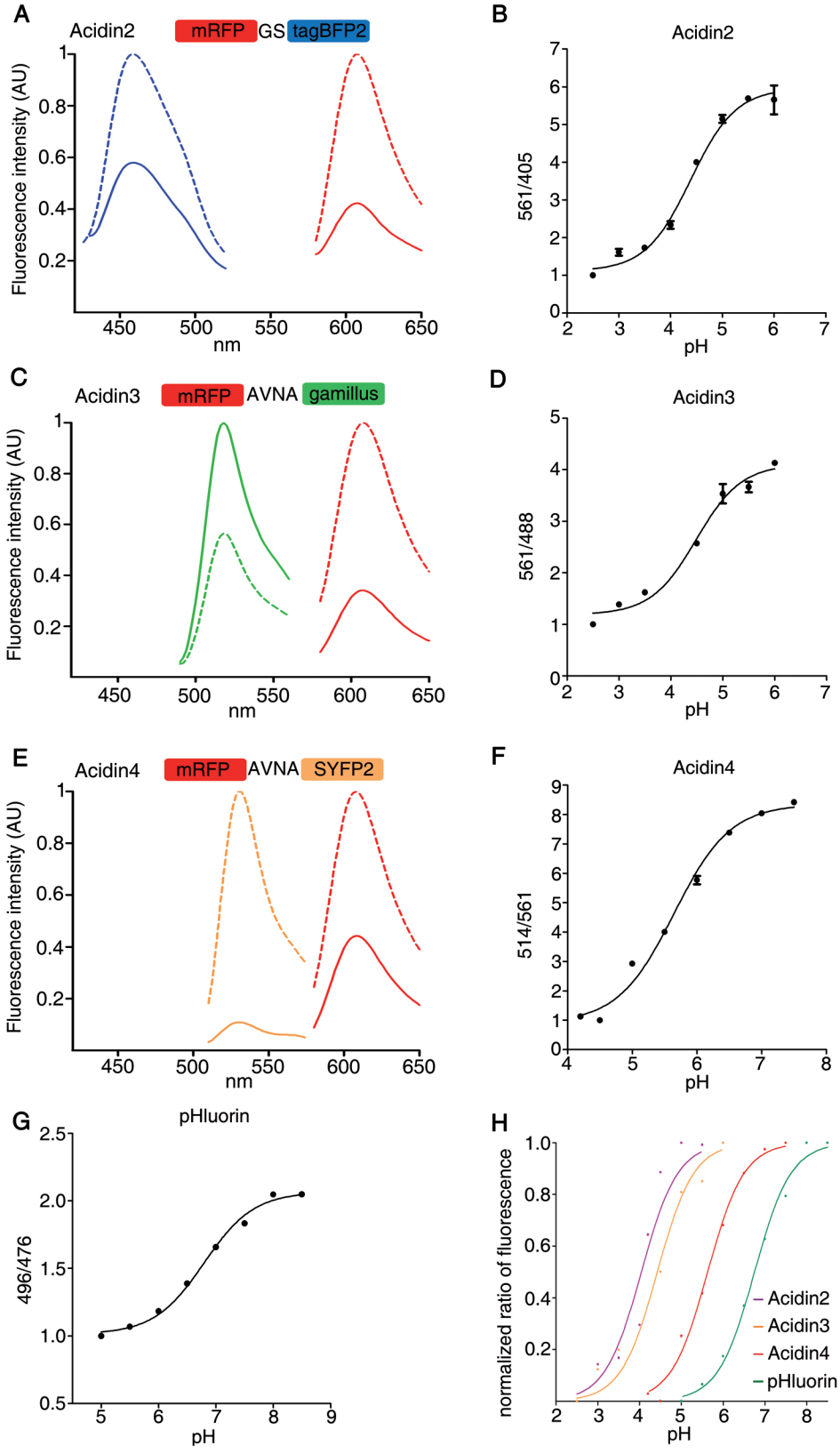


**Figure 1: Schematic representation and *in vitro* characterization of Acidins**

Acidin2 (A and B), Acidin3 (C and D) and Acidin4 (E and F) are genetically encoded tandems of fluorescent proteins made with mRFP (pKa 4.5) fused respectively to TagBFP2 (pKa 2.7), Gamillus (pKa 3.4), or SYFP2 (pKa 6) by a GS or AVNA linker. The Acidins were produced in *E. coli*, and their responses to pH were analyzed.

A, C and E: Emission profiles of the fluorescent proteins in Acidins at the highest (dashed line) or lowest pH (solid line) in the linear range of pH sensing. These values correspond to pH 5 and 2.5 for Acidin2, pH 5.5 and 2.5 for Acidin3, and pH 7 and pH 4.5 for Acidin4. Profiles obtained by spectrofluorometry are expressed in arbitrary units relative to the optimum and set to 1 for each fluorescent protein composing the tandem.

B, D, F and G: pH calibration curves for the three Acidins are represented as fluorescence ratios at the excitation wavelength ratios 561 nm/405 nm (B), 561 nm/488 nm (D), 514 nm/561 nm (F) and 496 nm/476 nm (G). Ratios obtained with a confocal are expressed relative to the minimum and set to 1 (see Fig. S3 for the raw data and details).

H: Normalized *in vitro* calibration curves of Acidins in comparison to pHluorin, fit with sigmoidal curves (Acidin2: $R^2 = 0.95$, pKa = 4.4; Acidin3: $R^2 = 0.96$, pKa = 4.5; Acidin4: $R^2 = 0.99$, pKa = 5.6; and pHluorin: $R^2 = 0.99$, pKa = 6.8). Data are transformed into the range 0-1 by Min-Max normalization.

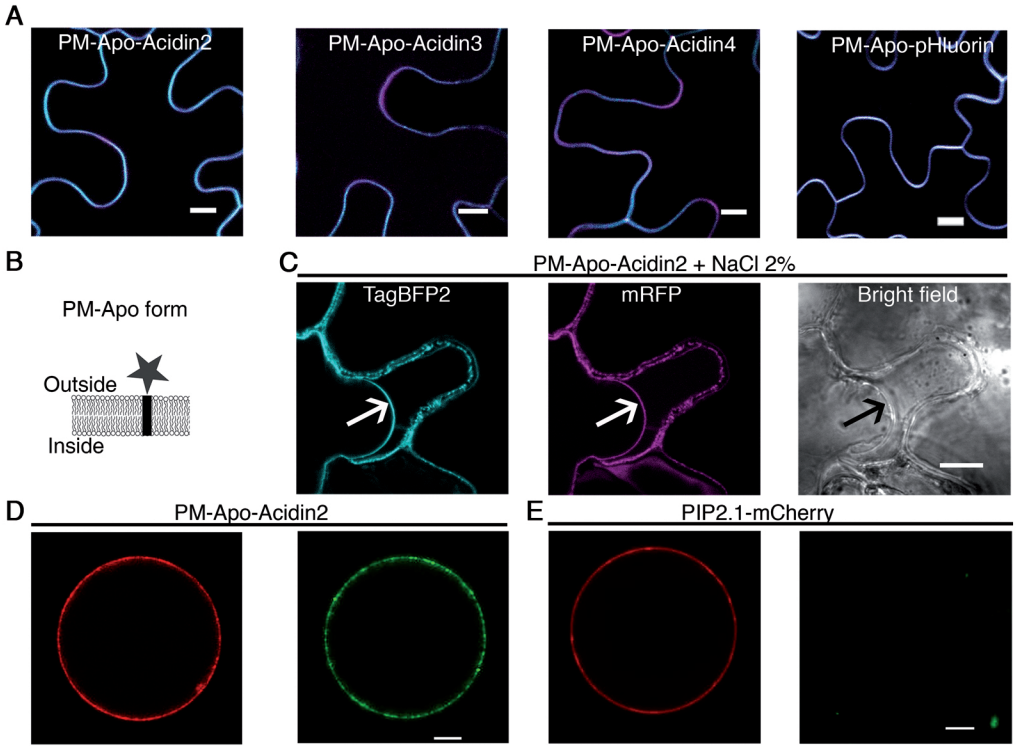


**Figure 2: Localization of PM-anchored Acidins in tobacco epidermal cells**

Tobacco epidermal cells were transiently transformed with pH sensors anchored in the PM. Cells were then analyzed after three days of expression with a confocal microscope.

A: Merge images showing the expression pattern of PM-Apo with either Acidin2, Acidin3, Acidin4 or pHluorin.

B: Schematic representation of the Acidin fusion protein PM-Apo.

C: Cells expressing PM-Apo-Acidin2 were submitted to plasmolysis with 2% NaCl for 30 min prior to observation.

D and E: Living tobacco protoplasts expressing either PM-Apo-Acidin2 (D) or the PM protein aquaporin PIP2.1 tagged on its cytoplasmic side with mCherry (E) were immunolabelled with rabbit primary anti-DsRed antibodies and secondary anti-rabbit Alexa Fluor 488 F(ab)'2 antibodies. In red: fluorescence emitted from either mRFP (D) or mCherry (E). In green: fluorescence signal resulting from immunolabelling was detected only for the PM-Apo-Acidin2 fusion (D), confirming the exposure of mRFP on the outside of the protoplast.

Cyan: fluorescence signal from TagBFP for Acidin2, Gamillus for Acidin3, SYFP2 for Acidin4, or 476Exc for pHluorin.

Magenta: fluorescence signal from mRFP for the Acidins, or the 496Exc channel for pHluorin. Arrow: PM. Scale bar: 10 µm.

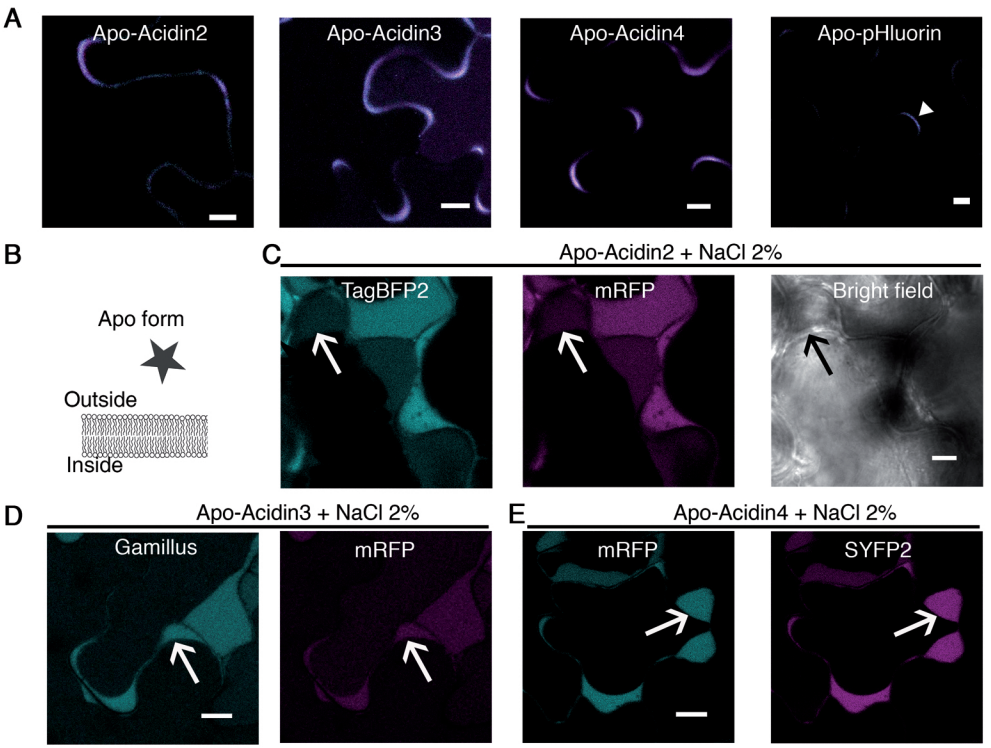


**Figure 3: Localization of free-diffusing apoplastic Acidins in tobacco epidermal cells**

Tobacco epidermal cells were transiently transformed with pH sensors released in the apoplast. Then, after three days of expression, cells were analysed with a confocal microscope.

A: Merge images showing the expression pattern of Apo with either Acidin2, Acidin3, Acidin4, or pHluorin.

B: Schematic representation of the Acidin fusion protein Apo.

C-E: Cells expressing either Apo-Acidin2 (C), Apo-Acidin3 (D) or Apo-Acidin4 (E) were submitted to plasmolysis with NaCl 2% for 30 min prior to observation.

Cyan: fluorescence signal from TagBFP for Acidin2, Gamillus for Acidin3, SYFP2 for Acidin4, or 476Exc for pHluorin. Magenta: fluorescence signal from mRFP for the Acidins, or the 496Exc channel for pHluorin. Arrowhead: labeled apoplast. Arrow: PM. Scale bar: 10 µm.

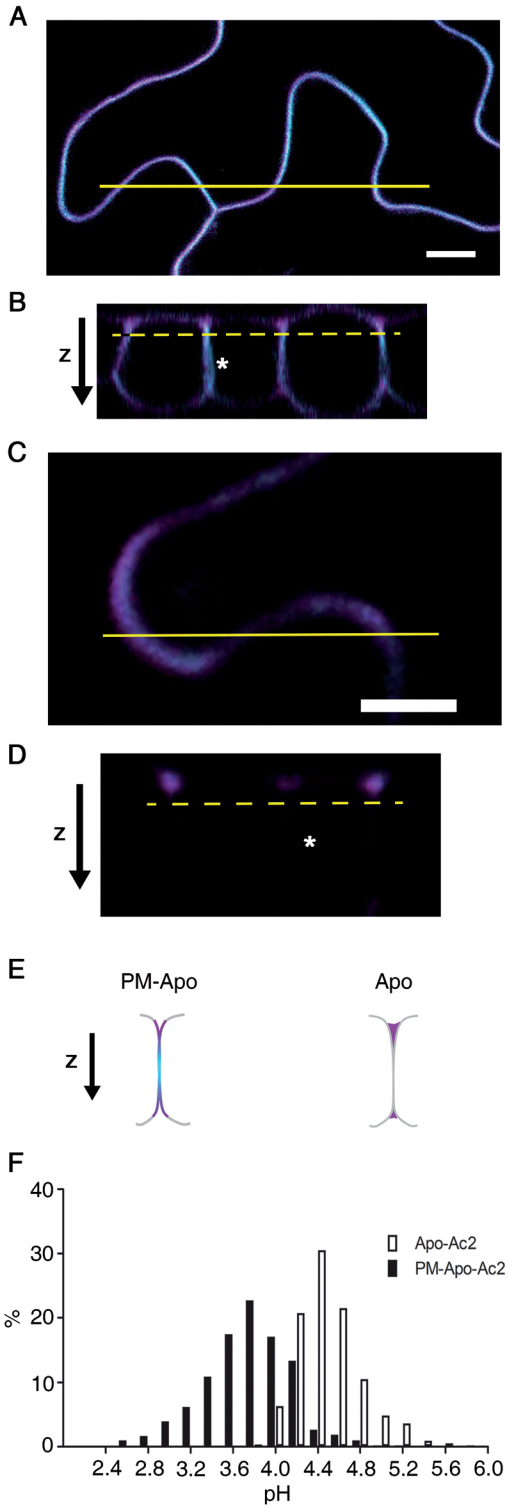


**Figure 4: Acidins reveal the existence of apoplastic subdomains with different pH values in tobacco epidermal cells**
Tobacco leaves transiently transformed with the sensor PM-Apo-Acidin2 (A and B) or Apo-Acidin2 (C and D) were observed under a confocal microscope. Series of confocal images were taken through the thickness of the epidermis from which a single focal plane is presented in a periclinal view (A and C) or an anticlinal view (B and D). The solid yellow line indicates the ROI from which the z projection was performed, whereas the dashed yellow line indicates the focal plane from which the respective periclinal view originated.
E: Schematic z projection of fluorescence labelling in pavement cell epidermis for PM-anchored (PM-Apo) and freely diffusing (Apo) forms of apoplastic fusions. PM-Apo labels the entire thickness of the epidermal PM, whereas Apo is restricted to the periclinal part of the apoplast.
F: Histograms of pH distribution collected from periclinal views for PM-Apo-Acidin2 (n = 568) or Apo-Acidin2 (n = 552).
False color: cyan for the TagBFP2 signal and magenta for the mRFP signal. Stars indicate the middle of the epidermal layer. Scale bar: 10 µm.

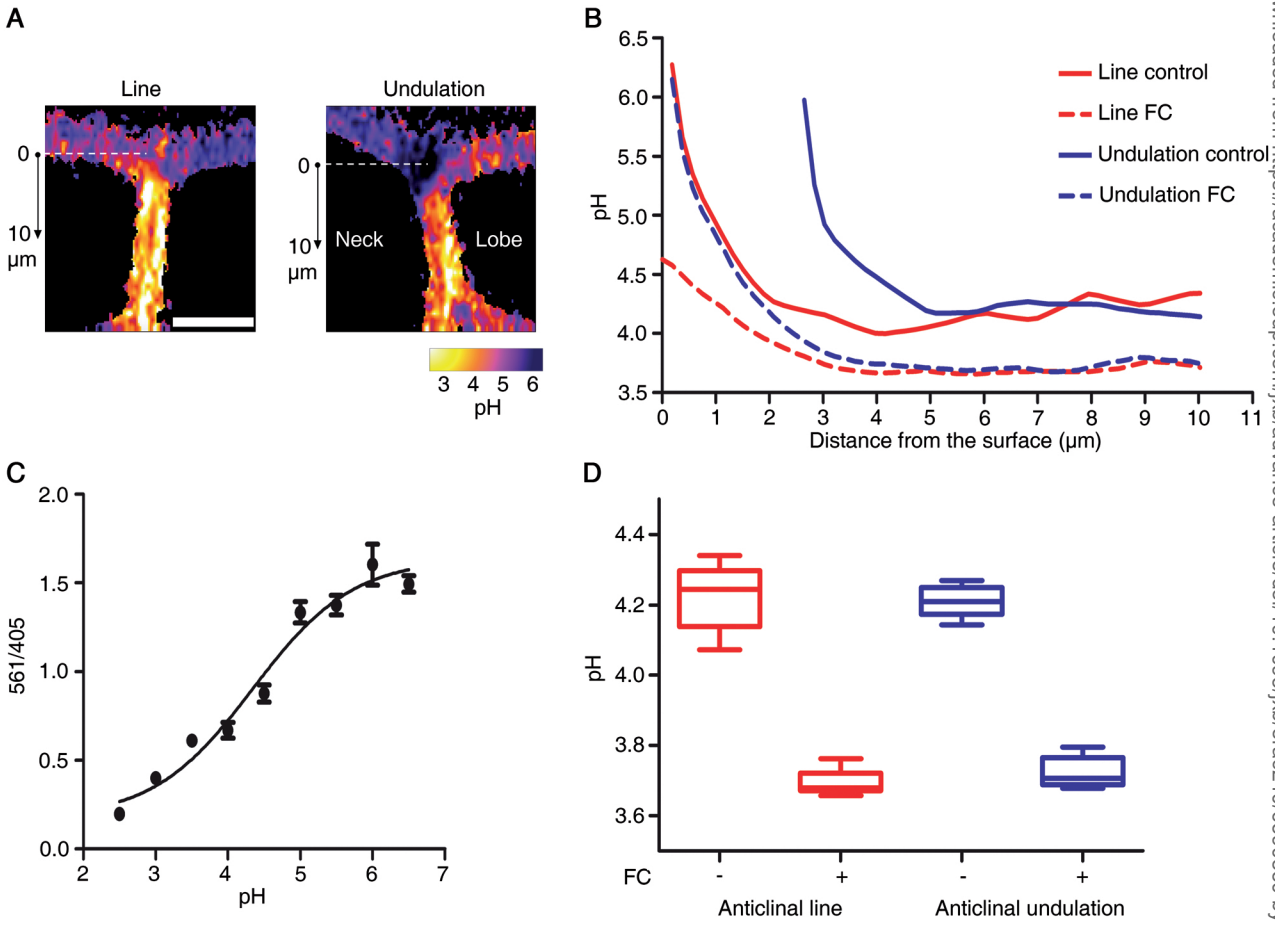


**Figure 5: PM H⁺-ATPase is involved in the acidification of the apoplast through pavement cell thickness**

Tobacco leaves transiently transformed with the sensor PM-Apo-Acidin2 were observed under a confocal microscope. Series of confocal images were taken through the thickness of the epidermis and z projections were generated in either undulated or straight regions of the cell periphery.

A: Ratiometric images of an anticlinal view in straight (line) or undulated (undulation) regions of pavement cells. The dashed white line indicates the zero position from which fluorescence data were collected for pH quantification through the epidermis thickness.

B: pH profile from the anticlinal-periclinal intersection (zero) up to 10 µm into the cell layer in straight (red) or undulated (blue) regions with (dashed line) or without (solid line) treatment with 10 µM fusicoccin.

C: *In vivo* calibration curve obtained from the z projection after clamping with nigericin at various pH levels.

D: Effect of fusicoccin on pH in the anticlinal region of the epidermis (5 to 10 µm from the surface). n=27; ANOVA followed by Tukey's test; $p<0.05$ between a and b groups.

Scale bar: 10 µm.

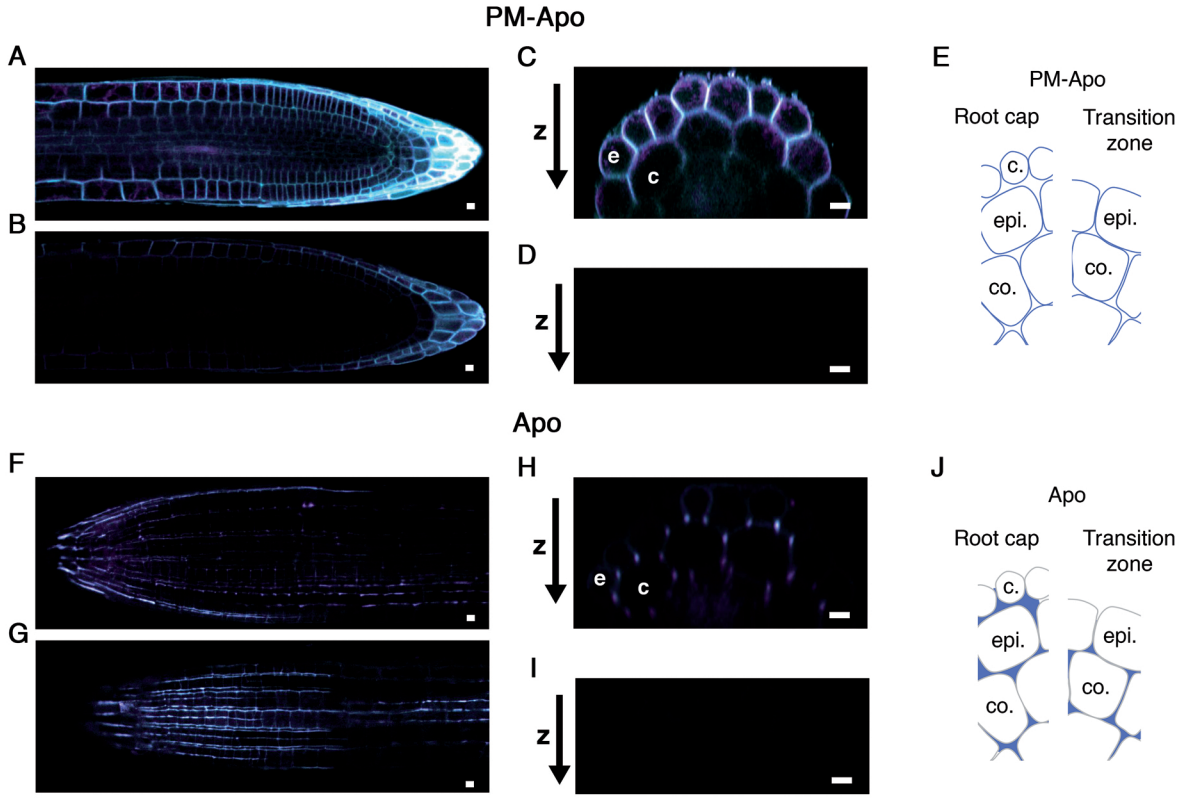


**Figure 6: Localization of Acidins in Arabidopsis primary root tip apoplast**

Primary roots from 5- to 6-day-old Arabidopsis seedlings expressing PM-Apo-Acidin4 (A-C) or Apo-Acidin2 (F-H) were observed with a confocal microscope.

A-B: Confocal merge images at a focal plane in the median section with high (A) or low (B) laser power.

C-D: Z projection in the transition zone of a PM-Apo-Acidin4 root (C) or an untransformed root at the same settings (D).

F-G: Confocal merge images at two different focal planes of the same root; see also Supplemental Movie 3 for the entire z-series.

H-I: Z projection in the transition zone of Apo-Acidin2 roots (H) or untransformed roots at the same settings (I).

E and J: Schematic z projections of the fluorescence pattern in primary roots for PM-anchored (PM-Apo; E) and freely diffusing (Apo; J) forms of apoplastic fusions showing that PM-Apo equally labels all cell layers, whereas Apo is accumulated in pockets between cells and can be detected at the surface of the epidermis only when the root cap cell layer is present.

c: cap cell layer; e: epidermis; co: cortex. Scale bar: 10 µm.

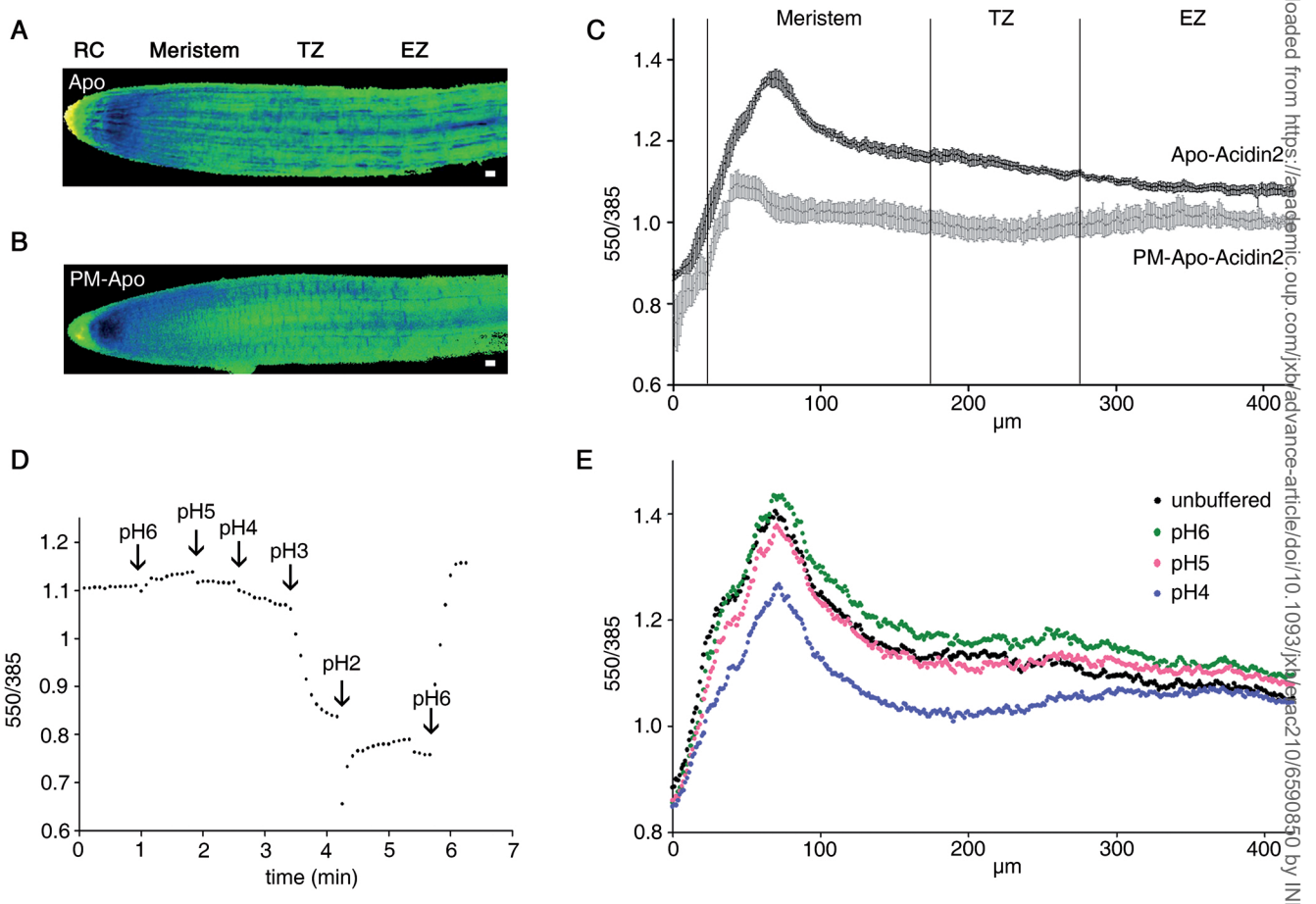


**Figure 7: Ratio of fluorescence monitoring and *in vivo* calibration in Arabidopsis root tips**

Arabidopsis plants were stably transformed with PM-Apo-Acidin2 and Apo-Acidin2 and fluorescence was observed in the primary roots of 5- to 6-day-old seedlings using ratiometric imaging.

A and B: Ratiometric images in false color of the first 400 µm (apical part) of primary root tips expressing either Apo-Acidin2 (A) or PM-Apo-Acidin2 (B).

C: Typical ratiometric profiles, with high values corresponding to high pH (n = 7 for Apo-Acidin2 and n = 3 for PM-Apo-Acidin2).

D and E: 561 nm/405 nm fluorescence ratio over time in the transition zone (D) or in the first 400 µm of the root tips expressing Apo-Acidin2 after equilibration (E) and perfusion with unbuffered half-strength MS, and then successively with half-strength MS buffered at various pH (100 mM glycine-HCl for pH 2 and pH 3, or 100 mM MES-KOH 0.1M for pH 4 to pH 6). See also Supplemental Movie 4.

RC: root cap; TZ: transition zone: EZ: elongation zone. Scale bar: 10 µm.

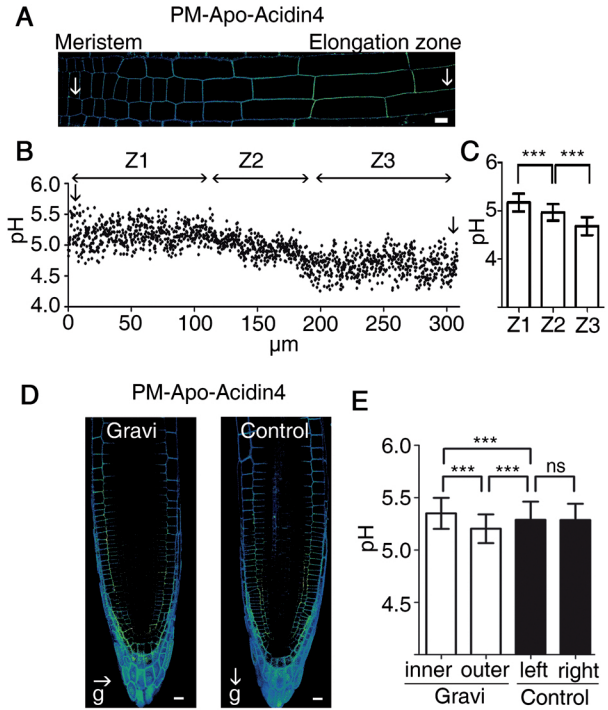


**Figure 8: pH variations monitored in living Arabidopsis primary roots expressing Acidins are associated with cell elongation**

Arabidopsis plants were stably transformed with PM-Apo-Acidin4 and fluorescence was observed in the primary roots of 5- to 6-day-old seedlings using a confocal microscope.

A and B: Ratiometric image from a 300-µm portion of the epidermis in the transition zone of a primary root tip (A) and the corresponding pH profile (B) from the intercellular portion delimited by arrows in A.

C: Measures of pH in the three zones identified in B ($pH_{Z1}$ = 5.1, n = 2,971; $pH_{Z2}$ = 5, n = 2,102; $pH_{Z3}$ = 4.6, n = 2,675, $p<0.0001$).

D: Ratiometric images of root tips from 5- to 6-day-old seedlings maintained in normal conditions (Control) or submitted to a 90° rotation for 25 to 30 min (Gravi).

E: pH measured in the epidermal cell layer at the outer and inner sides of the root after gravistimulation or at the left and right sides for the control root (n = 1,022 to 1,328, $p<0.0001$).